

Three-dimensional structure of the bacterial cell wall peptidoglycan

Samy O. Meroueh*, Krisztina Z. Bencze[†], Dusan Heseck*, Mijoon Lee*, Jed F. Fisher*, Timothy L. Stemmler[†], and Shahriar Mobashery*[‡]

*Department of Chemistry and Biochemistry, University of Notre Dame, Notre Dame, IN 46556-5670; and [†]Department of Biochemistry, Wayne State University School of Medicine, Detroit, MI 48201

Edited by Christopher T. Walsh, Harvard Medical School, Boston, MA, and approved January 18, 2006 (received for review November 29, 2005)

The 3D structure of the bacterial peptidoglycan, the major constituent of the cell wall, is one of the most important, yet still unsolved, structural problems in biochemistry. The peptidoglycan comprises alternating *N*-acetylglucosamine (NAG) and *N*-acetylmuramic disaccharide (NAM) saccharides, the latter of which has a peptide stem. Adjacent peptide stems are cross-linked by the transpeptidase enzymes of cell wall biosynthesis to provide the cell wall polymer with the structural integrity required by the bacterium. The cell wall and its biosynthetic enzymes are targets of antibiotics. The 3D structure of the cell wall has been elusive because of its complexity and the lack of pure samples. Herein we report the 3D solution structure as determined by NMR of the 2-kDa NAG-NAM(pentapeptide)-NAG-NAM(pentapeptide) synthetic fragment of the cell wall. The glycan backbone of this peptidoglycan forms a right-handed helix with a periodicity of three for the NAG-NAM repeat (per turn of the helix). The first two amino acids of the pentapeptide adopt a limited number of conformations. Based on this structure a model for the bacterial cell wall is proposed.

murein sacculus | bacterial envelope

The peptidoglycan scaffold of the bacterial cell wall is a repeating *N*-acetylglucosamine (NAG)-*N*-acetylmuramic disaccharide (NAM) [NAG-(β -1,4)-NAM] having a pentapeptide attached to the *D*-lactyl moiety of each NAM. This pentapeptide stem participates in an interglycan cross-linking reaction, thus creating the cell wall polymer. In contrast to the two other β -1,4-linked glycan biopolymers, cellulose (repeating glucose) (1–4) and chitin (repeating NAG) (5–7) for which the 3D structure is solved, the structure of the bacterial cell wall has remained elusive because of its complexity and the lack of pure and discrete segments for structural study (8–18). Herein we describe the 3D structure, determined in aqueous solution by NMR, of a 2-kDa synthetic NAG-NAM(pentapeptide)-NAG-NAM(pentapeptide) tetrasaccharide cell wall segment. The defining aspect of this structure is an ordered, right-handed helical saccharide conformation corresponding to three NAG-NAM pairs per turn of the helix. The structure of this peptidoglycan segment is the basis for a proposal for the structure of the bacterial cell wall polymer.

Results and Discussion

3D Structure of the Peptidoglycan. Because of the critical significance of the cell wall to bacterial survival, and the exploitation of the cell wall biosynthetic enzymes for the chemotherapeutic intervention of infections, many experimental and theoretical studies have addressed the cell wall structure. Despite diffraction studies carried out >30 years ago on cell wall extracted from bacteria, which strongly suggested that the peptidoglycan polymer possessed regular order (11), the 3D structure of the cell wall is not known. An excellent account of the historical development of the hypotheses for the cell wall structure is given by Dmitriev, Toukach, and Ehlers in their recent review (18). The major reason for the lack of progress is the absence of a pure

fragment of the cell wall, having both the peptide and disaccharide components of the peptidoglycan, for structural investigation. To address this limitation we completed the 37-step synthesis of such a segment (1, Fig. 1A) (19). The structure of this segment replicates a strand of the Gram-positive peptidoglycan (which has a L-Ala-D- γ -Glu-L-Lys-D-Ala-D-Ala pentapeptide stem), but replacement of the L-lysine by diaminopimelate would replicate the Gram-negative peptidoglycan structure. Compound 1 is sufficiently large to adopt discrete structure in solution, yet sufficiently small as to allow detailed NMR analysis at natural isotopic abundance.

Complete ¹H, ¹³C, and ¹⁵N assignments for 1 were made by correlation NMR (double quantum filtered-COSY, ¹H-total correlated spectroscopy, and ¹³C and ¹⁵N heteronuclear sequential quantum correlation) methods. A representative through-bond coupling experiment is shown in Fig. 2. A series of nuclear Overhauser effect (NOE) experiments were used to identify interatomic distance correlations that provided constraints used to solve the compound structure. Integrated peak volumes for each resonance, obtained at both 100- and 400-ns mixing times, were used to develop a build-up curve for subsequent distance restraints. A total of 63 independent ¹H-¹H NOE pairs (Tables 1 and 2, which are published as supporting information on the PNAS web site) were identified. Among these, 6 occur within the NAG-NAM disaccharide (3 NOEs between the NAG H-1 and NAM H-3 and 3 between the NAG H-1 and NAM H-4), 16 between the peptide and saccharide hydrogens, 13 between the peptide stem hydrogens, and the remainder between intrasaccharide hydrogens.

With the NOE restraints in place, a series of annealing molecular dynamics trajectories identified an ensemble of 20 conformations for 1 (Fig. 1B). In these conformations the two middle saccharides (NAM₁-NAM₂) show greater stability compared with the terminal (NAG₁ and NAM₂) saccharides. Three pairs of glycosidic dihedral angles define the tetrasaccharide conformation (where ϕ is the H₁-C₁-O₄-C₄ dihedral and ψ is the C₁-O₄-C₄-H₄ dihedral). For the conformations shown in Fig. 2B for 1, the three pairs of dihedral angles are (from left to right) $\phi_1 = 69 \pm 1^\circ$, $\psi_1 = 12 \pm 2^\circ$; $\phi_2 = 68 \pm 2^\circ$, $\psi_2 = 17 \pm 1^\circ$; and $\phi_3 = 66 \pm 8^\circ$, $\psi_3 = 16 \pm 7^\circ$. These angles are consistent with the preferred orientation of the C₄ carbon of NAM relative to C₂ and the ring oxygen of NAG along the C₁-O₄ bond as predicted by the *exo*-anomeric effect (20). In contrast to the defined tetrasaccharide conformation, the two pentapeptide stems show greater mobility. The *D*-Lac, L-Ala, and *D*-Glu of each adopt a limited

Conflict of interest statement: No conflicts declared.

This paper was submitted directly (Track II) to the PNAS office.

Abbreviations: NAG, *N*-acetylglucosamine; NAM, *N*-acetylmuramic disaccharide; NOE, nuclear Overhauser effect.

Data deposition: The NMR chemical shifts have been deposited in the BioMagResBank, www.bmrb.wisc.edu (accession no. 6992).

[‡]To whom correspondence should be addressed. E-mail: mobashery@nd.edu.

© 2006 by The National Academy of Sciences of the USA

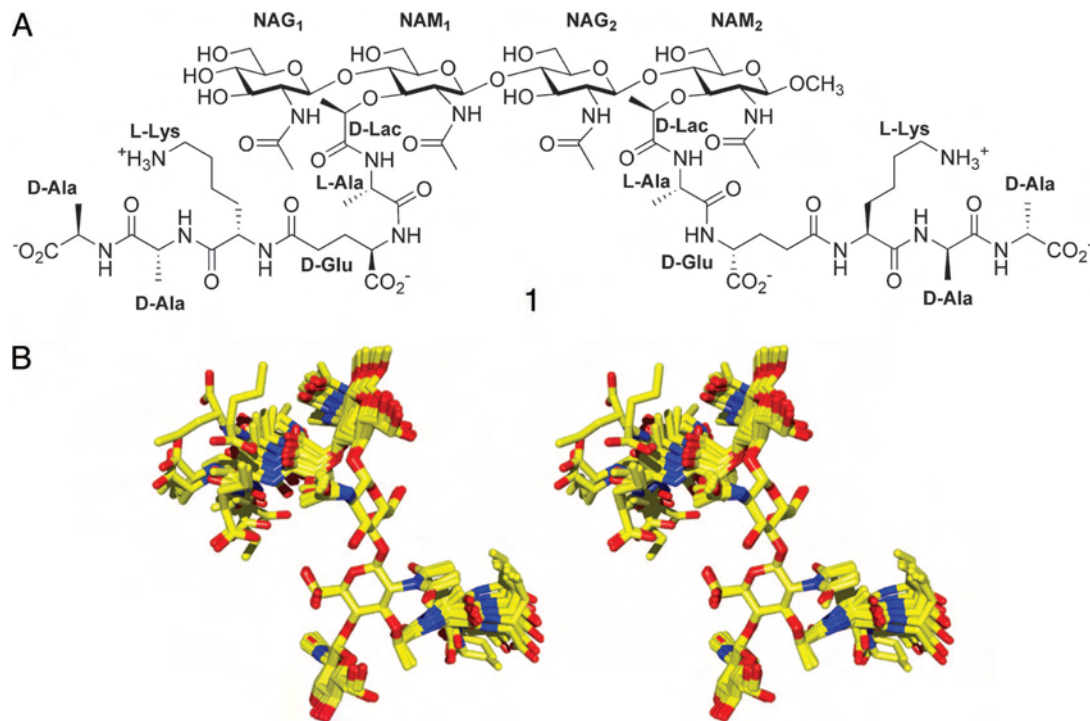


Fig. 1. Chemical structure and solution conformation of the peptidoglycan segment. (A) Chemical structure of compound 1. (B) NMR structure of the synthetic segment 1 of the cell wall, shown as a stereoview of 20 superimposed conformers. The disordered segments of the peptide stems (the L-Lys-D-Ala-D-Ala termini) are omitted for clarity. The conformers are depicted in capped sticks representation with O atoms in red, N atoms in blue, and C atoms in yellow.

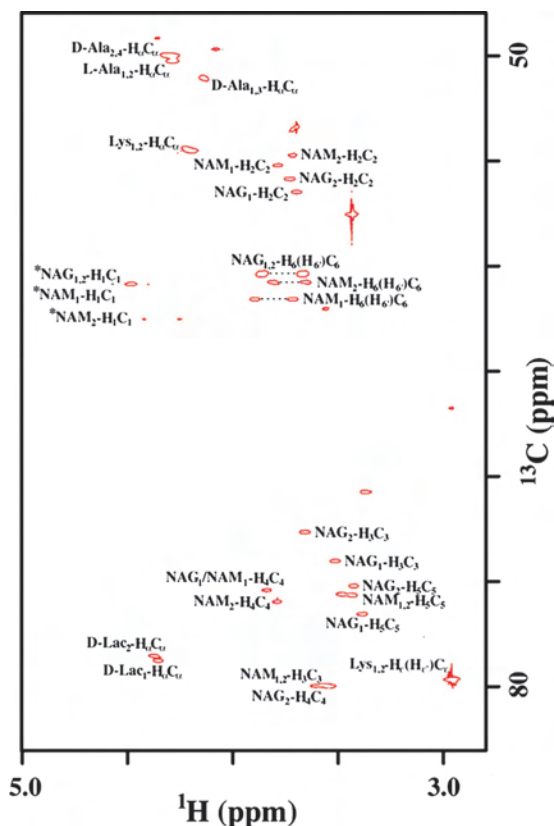


Fig. 2. The ^{13}C heteronuclear sequential quantum correlation spectrum of 1 showing ^{13}C correlations for the ^1H resonances between δ 2.8 and 5.0. This 600-MHz (with respect ^1H) spectrum was obtained at 298 K by using a 15-mM solution of 1 in 100% D_2O . Spectral features folded in the carbon dimension are identified by *.

number of conformers, whereas the L-Lys-D-Ala-D-Ala termini are disordered (that is, no NOE contacts are observed).

Early models ascribed a chitin-like structure to the bacterial peptidoglycan (8). Hence, the hydrogen-bond pattern that is observed in chitin was also presumed to occur in the bacterial peptidoglycan. In particular, a 2.7-Å intersaccharide hydrogen bond occurs in chitin between the pyranose oxygen and the C-3 hydroxyl moiety of the adjacent NAG rings. The structure determined for compound 1 shows, however, a distance between the pyranose oxygen of NAM and the C-3 hydroxyl oxygen of NAG of 3.4 Å. This distance is too long to be an important structural interaction. A second possible interaction in the peptidoglycan structure was proposed by Tipper (21). This structure features a hydrogen bond between the C-6 hydroxyl of NAG and the carbonyl oxygen of the lactyl group in NAM. The separation between these atoms in the 20 conformers of compound 1 is 8.2 Å, precluding the presence of this hydrogen bond. A third possible interaction was suggested by Knox and Murthy (22). This structure is characterized by a hydrogen bond between the lactyl moiety and the NAM acetamido nitrogen. This distance in the NMR structure of compound 1 is 5.1 Å. Hence, and in contrast to each of these proposals, the solution structure for 1 has no important intersaccharide hydrogen bonds contributing to its solution structure. The solution structure of 1 is set apart from the known structures of chitin and cellulose, where intersaccharide hydrogen bonds impart stability to their structures. The importance of water molecules in structures of carbohydrates in solutions cannot be discounted (23). We acknowledge that specific water molecules in the structure of 1 might bridge heteroatoms to afford additional stability.

Structure of the Peptidoglycan Oligomer. The average length of the peptidoglycan of the Gram-negative *Escherichia coli* strain W7 is nine NAG-NAM repeats (24–26). The defined and repeating glycosidic torsion angles of 1 (two NAG-NAM repeats) allows

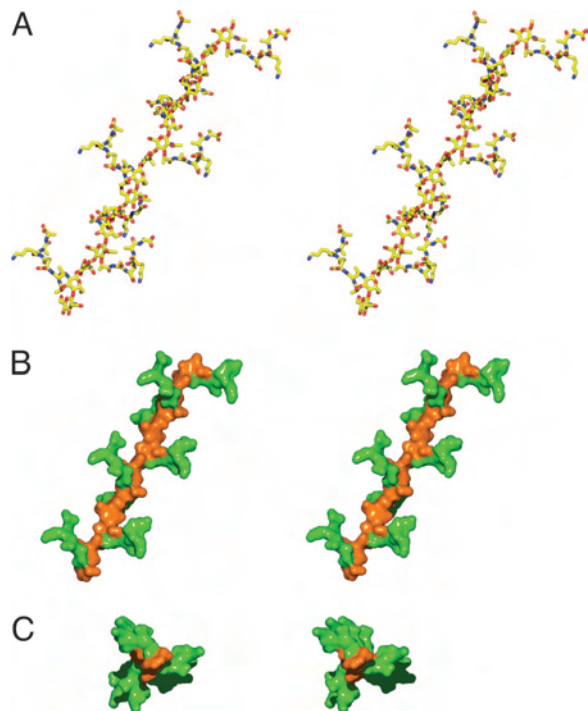


Fig. 3. The $[\text{NAG-NAM}]_8$ octamer construct derived from the NMR structure of 1. (A) Stereoview of a representative $[\text{NAG-NAM}]_8$ conformer, shown in capped-stick representation (O, N, and C are shown in red, blue, and yellow, respectively). (B) Solvent-accessible Connolly surface representation with the glycan backbone shown in orange and the peptide in green for the same perspective shown in A. (C) Stereoview of this construct seen from above (down the helical axis), shown as a solvent-accessible Connolly surface with the same the color coding as in B.

the prediction of the structure of the longer peptidoglycan. The result is a right-handed helix having three NAG-NAM repeats per turn (Fig. 3). Three-fold symmetry with respect to the peptide stems is seen with respect to the axis of the helix. This structure contrasts sharply with that of α -chitin, which has a 2-fold screw axis in which the planes of the saccharide rings orient at 180° to each other. This symmetry signifies that a lactyl-pentapeptide stem, attached to C-3 on the alternating saccharides of a peptidoglycan in the chitin conformation, will orient these stems to only one side of the axis. This outcome also applies to a cellulose glycan structure, as its structure is identical to that of chitin.

Structure of the Bacterial Cell Wall. The implication of the 3-fold symmetry adopted by the peptidoglycan is profound. Each strand of the peptidoglycan is predisposed for cross-linking to a maximum of three neighboring peptidoglycan strands. The extent of peptidoglycan cross-linking observed in bacteria is variable, and for *E. coli* is estimated to be $>40\%$ (26, 27). Hence not all strands are expected to cross-link. Using the expectation of incomplete cross-linking, the *in silico* generation of a larger cell wall segment was done. The result is the honeycomb pattern shown in Fig. 4 A and B. The smallest pores (three intact cross-links) are $\approx 70 \text{ \AA}$ across. This pore is large enough to contain, within its perimeter, the enzyme catalysts of its biosynthesis. As is evident from Fig. 4B, missing cross-links result in larger pores and missing strands result in even larger pores. The approximate diameter of a pore with one absent cross-link is 120 \AA . This honeycomb pattern agrees well with atomic force microscopic images of the Gram-positive bacterium *Staphylococcus aureus*, which show a surface dotted with pores ranging in size from 50 to 500 \AA (28).

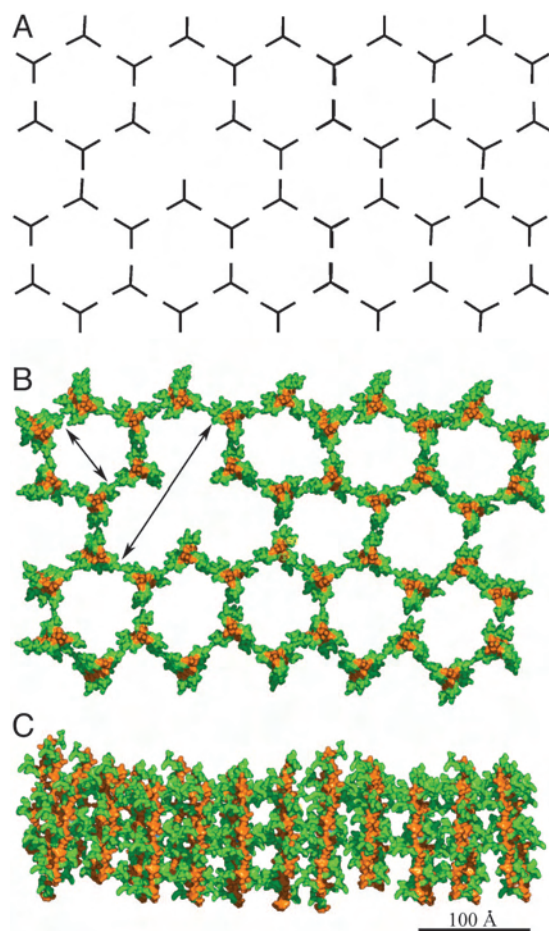


Fig. 4. Structure of the polymeric peptidoglycan segment. (A) Schematic of the top view of the structure of the cell wall with each peptidoglycan strand represented as a three-pronged star, mimicking the image shown in B. (B and C) Top (B) and side (C) views of the extended model of the structure of the cell wall. A Connolly solvent-accessible surface is used, showing the glycan strands in orange and the peptide stems in green (as also depicted in Fig. 3B for an individual strand of peptidoglycan). The top view is shown to a depth of eight NAG-NAM repeats, and double-headed arrows span a small and a larger pore. The longest strands in the side view are also eight NAG-NAM repeats. For reference, as determined by Matias *et al.* (42) the approximate thickness of the cell wall components for *E. coli* are: plasma membrane, 58 \AA ; peptidoglycan, 64 \AA ; periplasm, 210 \AA ; outer membrane (having a truncated lipopolysaccharide), 69 \AA .

The fundamental events of peptidoglycan biosynthesis are transglycosylase-catalyzed glycan lengthening and transpeptidase-catalyzed peptidoglycan cross-linking. These two reactions are often catalyzed by a single membrane-bound bifunctional enzyme, called the class A penicillin-binding protein (PBP) because of the ability of penicillin to inactivate (by irreversible acylation) its transpeptidase active site. The structure of this enzyme suggests that the two active sites of this PBP, the membrane-proximal transglycosylase and the membrane-distal transpeptidase, may be separated by as much as 70 – 100 \AA (29–31). The membrane proximity of the transglycosylase active site suggests that for a given peptidoglycan segment glycan strand extension precedes transpeptidase cross-linking. This presumption is supported by the observation (in the Gram-positive R61 transpeptidase) of two channels that cross the transpeptidase active site so as to accommodate entering and departing glycans for the two separate strands undergoing the cross-link (31). The ≈ 20 - \AA distance between the two grooves is consistent with this model.

peptidoglycan structures of Figs. 3–5 incorporate the solution structure of **1**, are consistent with expectations for architectural strength, and are attractive by several experimental criteria that define the cell wall structure. This structure is presented as a compelling hypothesis to guide further study of peptidoglycan biosynthesis and peptidoglycan interaction with the lipid and protein ensembles of the bacterial cell wall.

Methods

NMR Spectroscopy. NMR spectra were acquired by using a 15-mM solution of **1** (Chemical Abstracts Service Registry No. 678159-02-9) in either 9:1 H₂O/D₂O or D₂O, in the absence of added salt or buffer. The pH of these solutions was 4.4. NMR spectra were acquired at 25°C by using pulsed-field gradients on the following spectrometers: Varian INOVA 600-MHz spectrometer (Wayne State University), a Bruker (Billerica, MA) AVANCE 700-MHz spectrometer (Wayne State University), and a Varian INOVA 720-MHz spectrometer (National High Magnetic Field Laboratory, Tallahassee, FL). Spectral assignments were made by using double quantum filtered-COSY, total correlated spectroscopy, ¹³C-heteronuclear sequential quantum correlation (HSQC), and ¹⁵N-HSQC experiments. Distance constraints for structure calculations were obtained from a series of homonuclear 2D watergate-NOESY spectra at mixing times ranging from 100 to 400 ms (44). All spectra were collected with 4,096 points in the acquisition dimension (signal averaging with 4, 8, or 16 scans) and 128, 256, 400, or 512 points in the indirect dimension. Data were zero filled to 2K × 1K or 2K × 512 points before Fourier transformation. Spectra were referenced at each field by using an external 2,2-dimethylsilapentane-5-sulfonic acid standard sample.

Data were transformed by using FELIX 2000 (Accelrys, Inc., San Diego) and NMRPIPE (45). Peak identification and analysis were done by using the XEASY and SPARKY programs (46, 47). Approximate interproton distance restraints were derived in SPARKY from NOESY spectra, using a Gaussian volume integration methodology. On the basis of NOE build-up curves, the peaks were then grouped into three distance ranges of 1.9–2.5 Å, 2.5–3.7 Å, and 3.7–5 Å, corresponding to strong, medium, and weak NOEs, respectively (48).

Computational Methods. The 3D structure of **1** was constructed with the SYBYL 6.91 suite of programs. NOEs were then applied in the form of restraints: interproton distance ranges corresponding to short, medium, and long NOEs were restrained based on the aforementioned values. The molecule was prepared for NOE-restrained molecular dynamics simulations. Ensemble-averaged restrained electrostatic potential (RESP) charges were determined for each ring. This process consisted of subjecting the ring to a short molecular dynamics simulation, collecting 25 snapshots, determining the atomic charge of each snapshot by using the RESP methodology, and finally averaging the charges over all snapshots. Atomic charges for the peptide were determined in the same manner. Parameters for the carbohydrate portion of the molecule were obtained from GLYCAM04, which is

a specialized set of parameters, derived for the accurate simulation of carbohydrates. The rest were treated with parameters from the PARM99 data set that is part of the AMBER 7 suite of programs (49). For the simulated annealing runs, the solvent was treated implicitly as a dielectric continuum by using the Generalized-Born approach (50, 51). An initial annealing simulation was carried out for several 5-ns periods at 2,000 K, and a series of snapshots served as initial coordinates for subsequent annealing runs. A total of 540 simulated annealing trajectories were carried out. Each consisted of three rounds of the following sequence. The molecule was heated to 2,000 K for 10 ps, followed by 25 ps of dynamics at 2,000 K, and 25 ps of cooling to 0 K. The final cooling step was carried out for 375 ps. This sequence gave a total of 530 ps for each run and a combined 286 ns of simulation for all 540 trajectories. Each conformer was subjected to 10,000 steps of conjugate gradient energy minimization upon completion of the annealing run, and restraint violation energy was determined for each of the resulting energy-minimized structures. The structures were ranked based on the restraint violation energy. The 50 conformers with the smallest violation energy were superimposed along the carbon and oxygen atoms of the saccharide rings. Fig. 1B depicts the 20 structures having the smallest pairwise rms deviation.

To construct the structure of [NAG-NAM]₈ from that of the experimentally determined 3D structure of compound **1**, we used the program SYBYL 7.0 (Tripos Associates, St. Louis). The structure extension was performed with one addition of compound **1** to the nascent model at a time with the ϕ and ψ angles for the glycosidic torsions conforming to the experimentally determined values. At each step this was followed by an energy minimization using the SYBYL TRIPOS force field with Gasteiger charges. This procedure was repeated until the peptidoglycan helix contained eight NAG-NAM repeats. The program PYMOL (www.pymol.org) was then used to create multiple copies of the helix, which were positioned relative to each other based on the 3-fold symmetry of the helix and the current understanding of how the peptide stems are cross-linked by transpeptidases based on available x-ray coordinates. The 3D structure of TolC (Protein Data Bank ID code 1EK9) was obtained from the Research Collaboratory for Structural Bioinformatics database (www.rcsb.org). The structure was then docked into one of the small pores of the cell wall model by using SYBYL 7.0. Twenty thousand steps of steepest decent energy minimization were subsequently carried out by using the TRIPOS force field with Gasteiger charges, followed by a series of alternating short (10 ps) molecular dynamics simulations and additional energy minimization steps to equilibrate the system.

NMR Data. The NMR data for **1** are summarized by peak assignments with the NOE contacts (Table 1) and the peptide backbone torsion angles (Table 2).

This work was supported by National Institutes of Health Grants GM61629 and AI33170. The Varian INOVA 600-MHz NMR spectrometer was purchased with funds from National Institutes of Health Grant RR16627.

- Baker, A. A., Helbert, W., Sugiyama, J. & Miles, M. J. (2000) *Biophys. J.* **79**, 1139–1145.
- Nishiyama, Y., Sugiyama, J., Chanzy, H. & Langan, P. (2003) *J. Am. Chem. Soc.* **125**, 14300–14306.
- Klemm, D., Heublein, B., Fink, H. P. & Bohn, A. (2005) *Angew. Chem. Int. Ed.* **44**, 3358–3393.
- Ford, Z. M., Stevens, E. D., Johnson, G. P. & French, A. D. (2005) *Carbohydr. Res.* **340**, 827–883.
- Germer, A., Mugge, C., Peter, M. G., Rottmann, A. & Kleinpeter, E. (2003) *Chem. Eur. J.* **9**, 1964–1973.
- Abotiz, N., Vila-Perello, M., Groves, P., Asensio, J. L., Andreu, D., Canada, F. J. & Jimenez-Barbero, J. (2004) *ChemBioChem* **5**, 1245–1255.
- Colombo, G., Meli, M., Canada, J., Asensio, J. L. & Jimenez-Barbero, J. (2005) *Carbohydr. Res.* **340**, 1039–1049.
- Formanek, H., Formanek, S. & Wawra, H. (1974) *Eur. J. Biochem.* **46**, 279–294.
- Burge, R. E., Fowler, A. G. & Reaveley, D. A. (1977) *J. Mol. Biol.* **117**, 927–953.
- Labischinski, H., Barnickel, G., Bradaczek, H. & Giesbrecht, P. (1979) *Eur. J. Biochem.* **95**, 147–155.
- Leps, B., Labischinski, H. & Bradaczek, H. (1987) *Biopolymers* **26**, 1391–1406.
- Holtje, J. V. (1998) *Microbiol. Mol. Biol. Rev.* **62**, 181–203.
- Koch, A. L. (1998) *Res. Microbiol.* **149**, 689–701.
- Koch, A. L. (2000) *Arch. Microbiol.* **174**, 429–439.
- Vollmer, W. & Holtje, J. V. (2004) *J. Bacteriol.* **186**, 5978–5987.
- Cabeen, M. T. & Jacobs-Wagner, C. (2005) *Nat. Rev. Microbiol.* **3**, 601–610.

17. Scheffers, D. J. & Pinho, M. G. (2005) *Microbiol. Mol. Biol. Rev.* **69**, 585–607.
18. Dmitriev, B., Toukach, F. & Ehlers, S. (2005) *Trends Microbiol.* **13**, 569–574.
19. Heseck, D., Lee, M. J., Morio, K. I. & Mobashery, S. (2004) *J. Org. Chem.* **69**, 2137–2146.
20. Tvaroska, I. & Bleha, T. (1989) *Adv. Carbohydr. Chem. Biochem.* **47**, 45–123.
21. Tipper, D. J. (1970) *Int. J. System. Bacteriol.* **20**, 361–377.
22. Knox, J. R. & Murthy, N. S. (1974) *Acta Crystallogr. B* **30**, 365–371.
23. Kirschner, K. N. & Woods, R. J. (2001) *Proc. Natl. Acad. Sci. USA* **98**, 10541–10545.
24. Harz, H., Burgdorf, K. & Holtje, J. V. (1990) *Anal. Biochem.* **190**, 120–128.
25. Koch, A. L. (2000) *J. Theor. Biol.* **204**, 533–541.
26. Glauner, B. (1988) *Anal. Biochem.* **172**, 451–464.
27. Glauner, B., Holtje, J. V. & Schwarz, U. (1988) *J. Biol. Chem.* **263**, 10088–10095.
28. Touhami, A., Jericho, M. H. & Beveridge, T. J. (2004) *J. Bacteriol.* **186**, 3286–3295.
29. Lim, D. & Strynadka, N. C. (2002) *Nat. Struct. Biol.* **9**, 870–876.
30. Macheboeuf, P., Di Guilmi, A. M., Job, V., Vernet, T., Dideberg, O. & Dessen, A. (2005) *Proc. Natl. Acad. Sci. USA* **102**, 577–582.
31. Lee, W., McDonough, M. A., Kotra, L., Li, Z., Silvaggi, N. R., Takeda, Y., Kelly, J. A. & Mobashery, S. (2001) *Proc. Natl. Acad. Sci. USA* **98**, 1427–1431.
32. Akama, H., Kanemaki, M., Yoshimura, M., Tsukihara, T., Kashiwagi, T., Yoneyama, H., Narita, S., Nakagawa, A. & Nakae, T. (2004) *J. Biol. Chem.* **279**, 52816–52819.
33. Koronakis, V., Sharff, A., Koronakis, E., Luisi, B. & Hughes, C. (2000) *Nature* **405**, 914–919.
34. Koronakis, V., Eswaran, J. & Hughes, C. (2004) *Annu. Rev. Biochem.* **73**, 467–489.
35. Fernandez-Recio, J., Walas, F., Federici, L., Venkatesh Pratap, J., Bavro, V. N., Miguel, R. N., Mizuguchi, K. & Luisi, B. (2004) *FEBS Lett.* **578**, 5–9.
36. Tamura, N., Murakami, S., Oyama, Y., Ishiguro, M. & Yamaguchi, A. (2005) *Biochemistry* **44**, 11115–11121.
37. Lambert, O., Benabdelhak, H., Chami, M., Jouan, L., Nouaille, E., Ducruix, A. & Brisson, A. (2005) *J. Struct. Biol.* **150**, 50–57.
38. Dmitriev, B. A., Ehlers, S. & Rietschel, E. T. (1999) *Med. Microbiol. Immunol.* **187**, 173–181.
39. Dmitriev, B. A., Toukach, F. V., Schaper, K. J., Holst, O., Rietschel, E. T. & Ehlers, S. (2004) *J. Bacteriol.* **185**, 3458–3468.
40. Dmitriev, B. A., Toukach, F. V., Holst, O., Rietschel, E. T. & Ehlers, S. (2004) *J. Bacteriol.* **186**, 7141–7148.
41. Beveridge, T. J. (1999) *J. Bacteriol.* **181**, 4725–4733.
42. Matias, V. R., Al-Amoudi, A., Dubochet, J. & Beveridge, T. J. (2003) *J. Bacteriol.* **185**, 6112–6118.
43. Matias, V. & Beveridge, T. (2005) *Mol. Microbiol.* **56**, 240–251.
44. Cavanagh, J., Fairbrother, W., Palmer, A. G., III & Skelton, N. J. (1995) *Protein NMR Spectroscopy: Principles and Practice* (Academic, San Diego).
45. Delaglio, F., Grzesiek, S., Vuister, G. W., Zhu, G., Pfeifer, J. & Bax, A. (1995) *J. Biomol. NMR* **6**, 277–293.
46. Bartels, C., Xia, T.-H., Billeter, M., Guntert, P. & Wuthrich, K. (1995) *J. Biomol. NMR* **6**, 1–10.
47. Goddard, T. D. & Kneller, D. G. (2002) SPARKY 3 (Univ. of California, San Francisco).
48. Wuthrich, K. (1986) *NMR of Proteins and Nucleic Acids* (Wiley, New York).
49. Case, D. A., Pearlman, D. A., Caldwell, J. W., Cheatham, T. E., III, Wang, J., Ross, W. S., Simmerling, C. L., Darden, T. A., Merz, K. M., Stanton, R. V., et al. (2002) AMBER 7 (Univ. of California, San Francisco).
50. Bashford, D. & Case, D. A. (2000) *Annu. Rev. Phys. Chem.* **51**, 129–152.
51. Roux, B. & Simonson, T. (1999) *Biophys. Chem.* **78**, 1–20.